Astron. Astrophys. 262, 587–596 (1992)

ASTRONOMY AND ASTROPHYSICS

Time evolution of arch filaments

G. Tsiropoula[1], A. A. Georgakilas[2], C. E. Alissandrakis[2] and P. Mein[3]

[1] Institute of Space Research, National Observatory of Athens, P.O. Box 20048, GR-11810 Athens, Greece
[2] Section of Astrophysics, Astronomy and Mechanics, Department of Physics, University of Athens, GR-15784 Athens, Greece
[3] Observatoire de Paris Meudon, Section d'Astrophysique, F-92195 Meudon Principal Cedex, France

Received December 17, 1991; accepted April 27, 1992

Abstract. We have studied the spatial structure and the temporal evolution of the velocity in active region arch filaments. The observations were obtained with the Multichannel Double Pass Spectrograph (MSDP) operating in Hα at the Pic du Midi Observatory. Line profiles were reconstructed and monochromatic images and Doppler shift velocities were derived over a two dimensional field of view. Using Beckers' cloud model we derived physical parameters, in particular the line of sight velocity. The arches showed the "classical" type of motion, with material moving towards the observer near the apex and away from the observer near the footpoints. Assuming a symmetric loop, we reconstructed the velocity vector along the arch filaments. The results are consistent with the picture where material is draining out of the filament, while the whole structure is ascending. In one case we observed changes in the geometry and the velocity vector; however, other arch filaments did not change appreciably in a time period of about 13.5 min. We also observed an interesting case of arch filament formation. It appeared as a dark feature near one footpoint and expanded towards the other with an apparent velocity of about 13 km s^{-1}; however, the velocity data showed descending motions at the location of the expanding footpoint.

Key words: lines: profile – sun: chromosphere – sun: activity

1. Introduction

The study of the development of chromospheric active regions is of major interest to solar physicists. According to the widely accepted view, activity occurs where magnetic flux emerges from subphotospheric layers. Observations confirm this picture indicating that there is a spatial correlation between enhanced chromospheric emission in plages or the network and the underlying photospheric magnetic fields. The first stage of an active region has a characteristic pattern known as Emerging Flux Region (EFR) (Zirin, 1972), which takes place on a variety of length and time scales. The flux rate emergence of ephemeral regions is ten times that of active regions, while the flux rate emergence of intra-network elements is hundred times that of ephemeral regions. The chromospheric manifestation of an EFR seen in Hα, when the flux exceeds 0.5 10^{20} to 1 10^{20} Mx, consists of two regions of opposite polarity connected by a system of roughly parallel, dark, arch-shaped structures which are well coaligned with the transverse photospheric field (Chou and Wang, 1987). These loop-like structures, which Bruzek (1967) called Arch Filament Systems (AFS), apparently trace the lines of force of the emerging magnetic field.

The magnetic lines of force expand after they emerge out of the photosphere. The rising magnetic arch traps the chromospheric material which drains down both ends (following gravitation) as the arch rises. This material, lifted up with the flux rope, scatters the background radiation producing these dark structures easily observable in Hα, while an enhanced brightness around both feet is often observed at the time of the flux emergence which indicates the presence of magnetic energy dissipation. As long as the feet are bright we know empirically that flux continues to emerge (Zirin, 1972). Through such studies we can hope to discover the nature of energy transfer and dissipation; it appears that there is a tight correlation between the chromospheric heating rate and the photospheric field strength.

The AFS are replaced after 3 to 4 days by a system of arches called Field Transition Arches (FTA; Zirin, 1972). These are typical of the chromospheric structures which form in places where the magnetic field appears to be almost horizontal. There is no special brightening at the feet of FTA.

The dynamic characteristics and the physical parameters of AFS have been studied by Bruzek (1967, 1969), Roberts (1970), Frazier (1972), Chou and Zirin (1988), Alissandrakis et al. (1990), Georgakilas et al. (1990). The lifetime of an individual AF is estimated to be about 20 to 30 min (Bruzek, 1967); it undergoes, however, noticeable changes within 10 min. Arches continue to emerge until the flux stops rising and the entire system can be visible for several days. Individual arches in an AFS are fairly narrow, about 1000-3000 km, but there are arches which are not completely defined or are only incipiently resolved from their neighbours. The entire system can reach an extent of 25000 km, while the mean length of the arches is about 30000 km (extreme values 20000 - 40000 km) and their height goes up to 15000 km.

The velocity field is essential in understanding the emergence of magnetic flux. The observations show ascending motions near the apex with a velocity of 5 to 20 km s^{-1} and descending motions near both footpoints with a velocity of 35 to 50 km s^{-1} (Bruzek, 1969; Roberts, 1970; Zwaan, 1985; Chou and Zirin, 1988). Georgakilas et al. (1990), assuming a symmetric loop, reconstructed the velocity vector along an arch filament; they found ascending motions at ~10 km s^{-1} at the apex of the loop,

Send offprint requests to: G. Tsiropoula

descending motions at ~8 km s^{-1} near the footpoints as well as horizontal flows from the apex towards the footpoints. The picture that comes out of these observations is that material drains out of the rising flux tube. Another interesting quantity is the separation velocity of the footpoints, which is probably less than 1 km s^{-1}, a value reported by Chou & Wang (1987) who measured the separation velocity of emerging opposite poles of 24 new dipoles on the Sun.

Arch filaments are very important structures since, as has been pointed out, nearly all active regions begin as an AFS. They are related to the combined transport of matter and increasing magnetic field during the growth of the spotgroup. Thus the AFS could become excellent tools for charting the critical early stages of the evolution of magnetic fields on the solar surface. Our goal is to use a reasonably accurate, yet convenient method for determining the physical conditions within an arch and in particular the mass velocity and study their temporal evolution. This method has been used for this type of data (Alissandrakis et al., 1990) and is Beckers' cloud model (Beckers 1964). Compared to the results of Georgakilas et al. (1990), who derived the line of sight velocity from observations at Hα ±.5 Åusing plausible values for the optical depth and the Doppler width, the present results are more accurate since we use the entire Hα profile.

Table 1. Observations of AFS

Frame	Time (UT)	AFS in the field of view†			
		A	B	C	D
1	7:16:48	-	V, R	P	-
2	7:17:41	V	V, R	P	-
3	7:18:56	-	-	V, R	V, R
4	7:20:18	-	-	V, R	V, R
5	7:22:00	-	-	P	V, R
6	7:25:22	-	V, R	V, R	P
7	7:25:30	-	-	P	V
8	7:27:28	V	V, R	V, R	-
9	7:28:45	V	V, R	V, R	-
10	7:30:26	V	V, R	P	-
11	7:32:15	-	-	V, R	P

† V: Visible, P: Partly Visible, R: Used for reconstruction of the velocity vector

2. Derivation of physical parameters

The Sun's outer atmosphere is extremely complex and the underlying physical phenomena are far from being fully understood. The morphology and evolution of a given physical structure seen in the light of strong lines on the Sun is observed through the variation of the emerging radiation intensity, I(λ), which gives rise to a pattern of light and dark contrasts. The determination of the physical quantities from these disturbed line intensity (or contrast) profiles and in particular the determination of the temporal evolution of the velocity fields is an essential step in understanding the mechanisms of bulk plasma acceleration and energy transfer. However the derivation of fully consistent models that will correctly describe the variation of the intensity in terms of the physical parameters is a rather complicated problem which needs multi-dimensional solutions of the time-dependent non-LTE transfer equations.

Hα observations constitute a significant fraction of solar observations. They reveal a complex pattern of bright and dark features. In order to benefit from the large amount of information contained in these observations different methods have been proposed to account for the physical processes responsible for the observed patterns and to derive some physical parameters useful for the modelling of these features. The Hα intensity variation (as any line's intensity variation), arises from the variation in space and time of the source function S_λ and of the absorption coefficient, κ_λ. The absorption coefficient may be written in the form $\kappa_\lambda = \alpha_\lambda \phi(\lambda)$, where α_λ, the atomic absorption coefficient, depends only on atomic constants and the number density N_2 of hydrogen atoms in the second quantum level. The profile $\phi(\lambda)$ is a function of the Doppler width, $\Delta\lambda_D$, and the bulk velocity vector, v. The source function S_λ depends on the population ratio N_3/N_2, where N_3 is the number density of hydrogen atoms in the third quantum level. It is evident therefore that the morphology of Hα fine structures arises primarily from the 3-dimensional variation of N_2, N_3, v and $\Delta\lambda_D$.

To investigate further how variations in Hα structures depend on variations of these parameters it is convenient to distinguish between two different approaches concerning the optical depth at line center τ_o : (1) optically thin structures in which $\tau_o < 1$ and (2) optically thick structures which do not satisfy this requirement. Optically thick structures require the solution of the transfer equation together with the statistical equilibrium equations. The problem is simplified if we consider optically thin structures. Two kinds of optically thin models have been discussed in the literature: "embedded features" located inside the background chromosphere (Gebbie & Steinitz 1974; Steinitz et al. 1977) and clouds located above the background (Beckers 1964). This latter model, the "cloud" model, has been used extensively in the analysis of chromospheric absorption features seen in the Balmer lines (Grossmann-Doerth and von Uexkull 1971, 1973, 1977; Bray 1973, 1974; Bray and Loughhead 1983; Alissandrakis et al. 1990). This model assumes that the source function is frequency-independent and moreover that it is constant throughout the cloud and adopts a four parameter representation of the contrast profile:

$$C(\Delta\lambda) = \frac{I(\Delta\lambda) - I_o(\Delta\lambda)}{I_o(\Delta\lambda)} = \left(\frac{S}{I_o(\Delta\lambda)} - 1\right)\left(1 - e^{-\tau(\Delta\lambda)}\right)$$

where $I_o(\Delta\lambda)$ is the reference profile emitted by the background. In addition, one assumes that the wavelength dependence of the optical thickness is gaussian:

$$\tau(\Delta\lambda) = \tau_o e^{-\left(\frac{\Delta\lambda - \Delta\lambda_I}{\Delta\lambda_D}\right)^2}$$

and that the optical depth, τ_o, the Doppler shift, $\Delta\lambda_I$ and the Doppler width, $\Delta\lambda_D$ are constant throughout the cloud. The cloud model offers the attractive possibility of deriving several physical parameters of chromospheric features. However, only under a restricted range of circumstances (see Alissandrakis et al. 1990) do these parameters reflect accurately the atmospheric properties. The most basic of these is that only profiles of features lying at such a height that the Hα line is entirely formed below their lower boundary can be matched by this model. AFS are located at such a high level that one can assume safely that the Hα line is formed below the lower boundary of the structure.

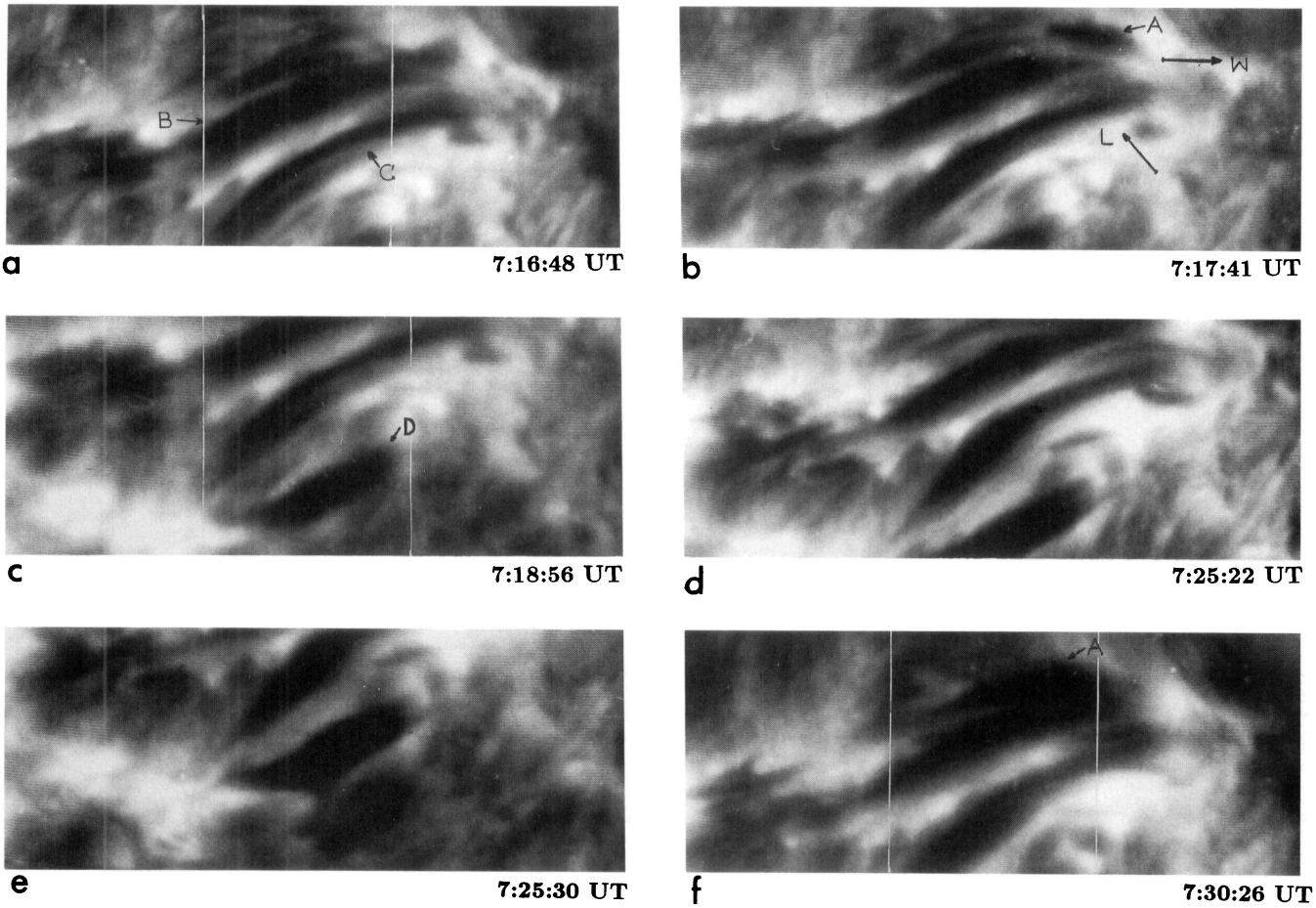

Fig. 1. Selected images of the AFS region at the center of Hα The white lines in (a), (c) and (f) mark the field of view of the cloud velocity maps in figures 3 to 5. The field of view is 75″ by 30″. The images are oriented with celestial North up. The arrow marked *L* shows the direction of the limb, while *W* points to the celestial west

Thus these structures are ideal for the application of the cloud model.

A common and widely used method to measure line-of-sight velocities is to determine the wavelength of a point midway between two positions of equal intensity in the absorption line profiles. This method is based on the assumption that the moving structure produces its own line profile, which is simply shifted with respect to the background profile by an amount $\Delta\lambda_I = \lambda v/c$. The determination of the velocities in this way is valid if the moving structure is located low enough so that the observed Hα profile is formed entirely within the structure (Bray 1974); if this is not true this method yields inconsistent results. As it is found by Alissandrakis et al. (1990), cloud velocities in AFS are about 2 to 5 times greater than Doppler velocities. They noticed, however, that the general behaviour is exactly the same e.g. positive or negative velocities given from the 2 methods were found at the same places.

3. Observations and data reduction

The present observations were made with the Multichannel Double Pass Spectrograph (MSDP) mounted on the 50 cm "Tourelle" refractor of the Pic du Midi Observatory. The MSDP records a two dimensional 4′ by 30″ field of the solar surface with good spatial (1″ by 1″) and temporal (10s) resolution (Mein, 1977, 1991). It provides 10 simultaneous intensity images of the same region, 0.256 Å apart in the Hα line. Because of the nature of the instrument, the position in the line profile is a function of the position in the field of view. From this set of data, maps of intensity fluctuations and Doppler shifts can be derived. By displacing the entrance slit, a large field of view (4′ by 2′ 30″) can be obtained each 60s. The region of the AFS was covered with two 4′ by 30″ elementary fields of view.

The observations of the AFS region (Active Region NOAA 4819, at N20E20) were made on June 22, 1987 covering a time interval of 15 m 27 s. From the entire sequence a set of 11 frames was selected. The observation time for each frame and the AFS inside the field of view are given in Table 1. Line profiles were reconstructed using the standard reduction methods for this type of data. Maps of intensity at the line center and Doppler velocities at +0.3 Å were computed from the profiles by a code simulating the "lambdameter" technique (Mein 1977). In addition, monochromatic images at +0.5 Å, −0.5 Å, +0.8 Å, and −0.8 Å were computed. The computation of the 4 parameters of the cloud model was carried out by an iterative least-square procedure for non-linear functions taking into account the restrictions described in Alissandrakis et al. (1990).

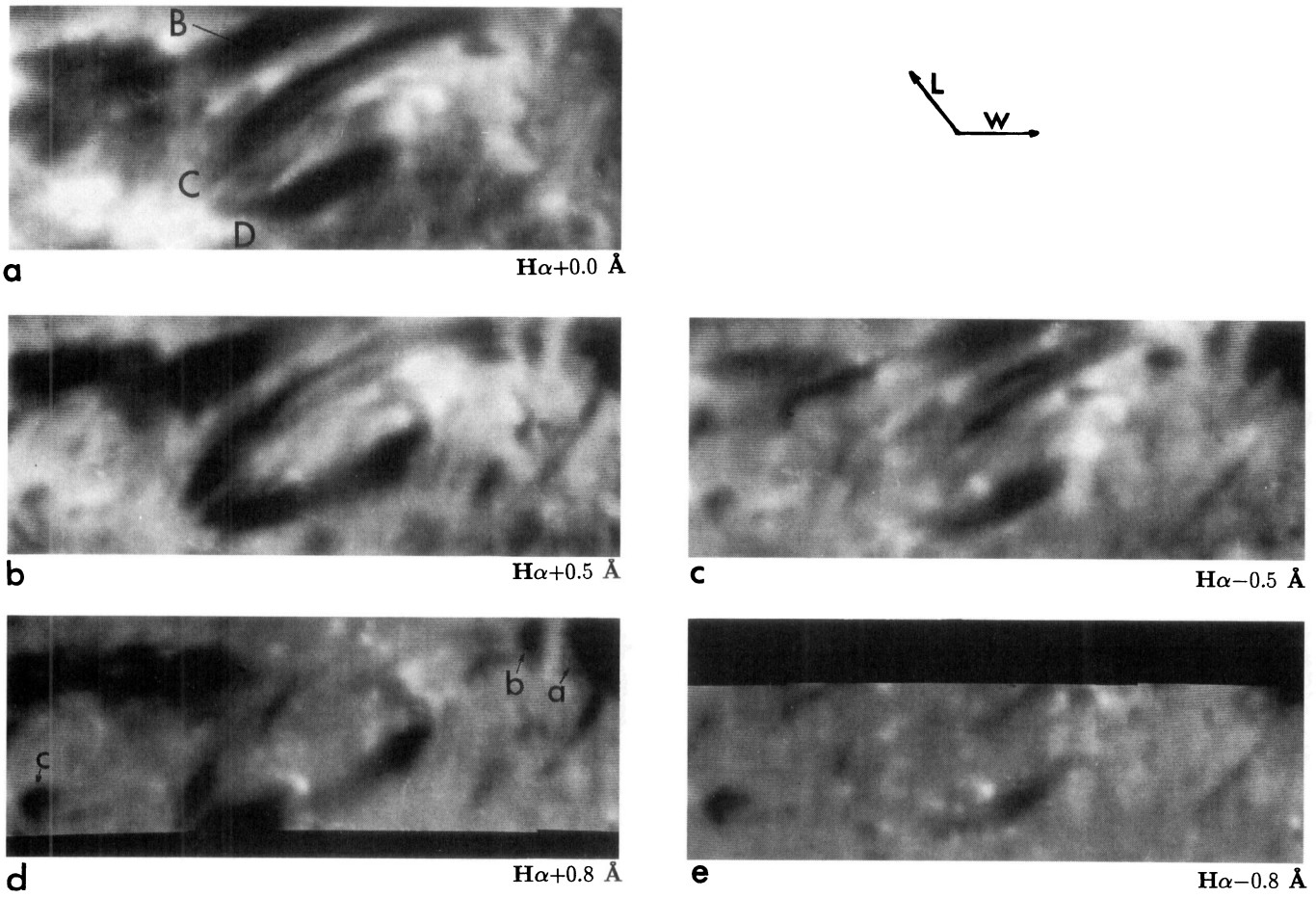

Fig. 2. The AFS region (7:18:56 UT) at five positions along the Hα profile. The arrow marked *L* shows the direction of the limb, while *W* points to the celestial west

4. Morphology and line-of-sight velocities

Figure 1 shows selected photographs of the AFS region at Hα center, covering a period of 13.5 minutes. The figure shows four bunches of arches, labeled *A* to *D*; each bunch consists of several individual filaments, some of which are unresolved. The field of view changes due to pointing difficulties, thus not all bunches are visible in every frame (cf. Table 1).

Figure 2 shows the same AFS region at five positions along the Hα profile. Bunches *C* and *D* are visible along their full length; in both, only the region near the apex appears at Hα −0.5 Å, whereas the footpoints are more intense at Hα +0.5 Å. An even smaller portion of the region near the apex appears at Hα −0.8 Å, whereas at Hα +0.8 Å we observe only the region near the footpoints. This pattern of positive Doppler shifts near the footpoints and negative Doppler shifts near the apex shows that the bunches have the "classical" type of motion. Individual arch filaments within the bunches are better visible in these photographs. We can also see the spots associated with the AFS, which are particularly prominent at Hα −0.8 Å (Fig. 2d). The spot *a* is the major leading spot; spot *b* is located just at the end of the west footpoint of bunch *C*, while another spot (marked *c* in Fig. 2d) is visible at the other side of the neutral line of the magnetic field. In addition to the arch filaments, there is a large dark structure in the upper left part of the photographs, which is particularly prominent at the center of Hα and the red wing.

The general behaviour of the source function is about the same in all bunches; it has a smooth variation with a minimum value of 130 to 140 (in units of 1/1000 of the continuum intensity) near the center of each arch filament (cf Alissandrakis et al. 1990), while near the edge of the arches it is slightly above the value of the background intensity, which is equal to 170. Source function contours define an approximate central axis for each bunch. The Doppler width and optical depth maps show the behaviour already noticed by Alissandrakis et al (1990), i. e. regions of high Doppler width have low optical depth and vice versa. This is not surprising since:

$$\tau_o \propto N_2 L/\Delta\lambda_D$$

where L is the geometrical thickness of the structure and N_2 the number density of the second hydrogen level. The contour maps of the product $\tau_o \Delta\lambda_D$ show that this quantity varies little over the arch filaments. It has a smooth variation with a maximum value of 0.7 Å near the central axis of each arch, while near the edge of the arches decreases to 0.3 - 0.4.

Figures 3a, 4a, 5a show contour maps of the line of sight velocity, computed with the cloud model method. A comparison of the contour maps with the corresponding Hα maps (Figs 1a, 1c, 1f) shows that the actual arch filaments are more extended than the regions for which the cloud velocity is computed. This apparently means that only the central part of the filament satisfies the condition of "high cloud" (according to the criteria of

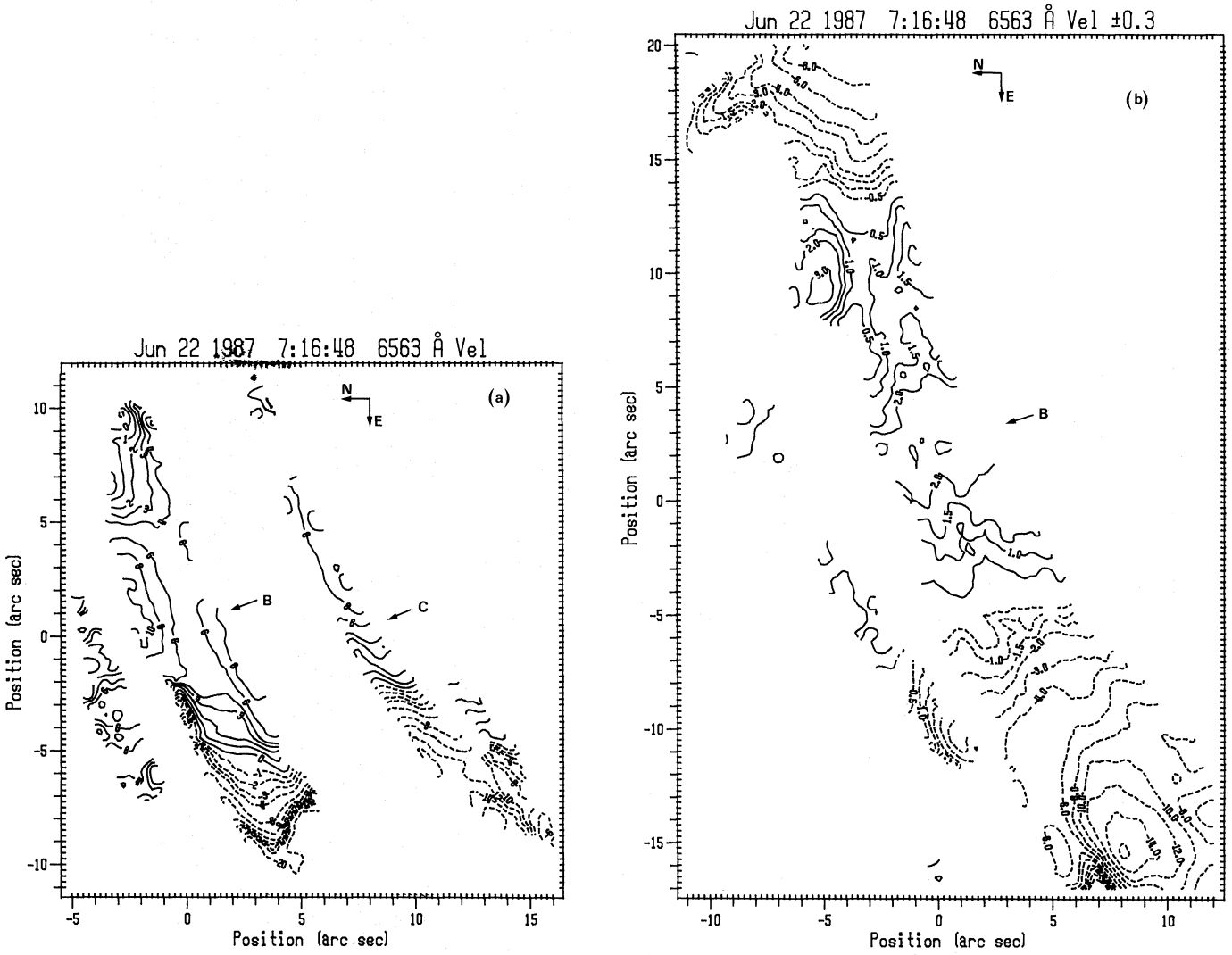

Fig. 3. Contour maps of cloud velocities (a) and Doppler velocities (b), at 7:16:48 UT. The maps are rotated by 90° with respect to Figs 1 and 2. Solid lines show motion towards the observer. Contour labels are in km s^{-1}

Alissandrakis et al. 1990). Contour maps of the velocity given by the Doppler shift method at Hα ±0.3 Å are shown in Figures 3b, 4b, 5b. An additional cloud map of the same region is given in Fig 3b of Alissandrakis et al. (1990), where the structures labeled *A*, *B* and *C* correspond to *B*, *C* and *D* of this work. The Doppler maps give no indication of the features or their boundaries (cf. Alissandrakis et al. 1990); therefore the boundaries of the arch filaments in the Doppler maps were determined by integrating the intensity over the Hα profile from −0.8 Å to +0.8 Å.

Comparing the velocity given by the cloud model and Doppler shift methods we note that the general behaviour is almost the same, e.g. positive or negative velocities are at about the same regions. On the other hand, Doppler shift computations provide too small velocity values (cf. Alissandrakis et al, 1990). It is interesting to note that the Doppler velocity maps show well defined peaks in the negative velocity region, near the edge of the AFS; this is particularly prominent in the east part of bunch *B*, in Fig. 3b. It is possible that these maxima represent the actual footpoints of the arches.

Bunches *B*, *C* and *D* are typical arch filaments which show the classical type of motion, with material ascending near the top and descending at the footpoints. Bunch *D* consists of at least two individual arches which overlap along almost all their length, except at their footpoints (Figs. 1, 2). The material moves towards the observer near the apex with a line-of-sight velocity of up to 6 km s^{-1} and away from the observer near the feet of the arch with a velocity larger than 10 km s^{-1} (Fig. 4a). From the position of the region on the solar disk, we conclude that these motions are ascending and descending respectively. We note that the motion does not have exactly the same properties in the two arches of the bunch, especially at the limbward part of the arch where the zero velocity contour is not perpendicular to the arch axis. This might be due to differences in the geometry of the individual arches (the south arch is a little shorter).

Both from the cloud and the Doppler maps we note that the velocity gradient along the axis of bunch D is smaller at the east (limbward) footpoint than at the west. Considering the position of the arch filament on the disk, this indicates horizontal motions towards the footpoints (cf. Georgakilas et al. 1990). During the 6.5 min that the bunch was in the field of view, it expanded

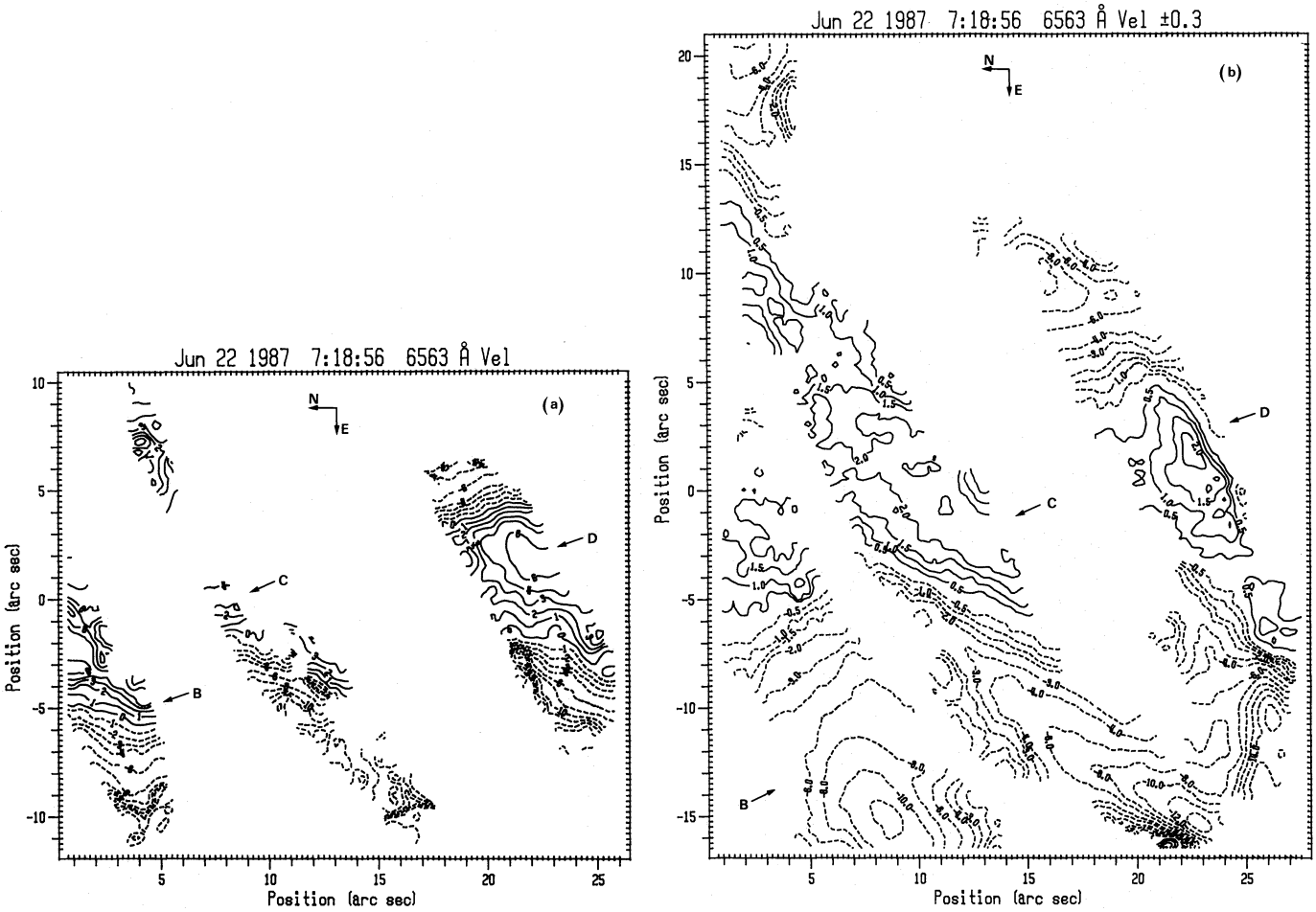

Fig. 4. Contour maps of cloud velocities (a) and Doppler velocities (b), at 7:18:56 UT

towards both footpoints, as seen at Hα center. At 7:16:48 UT its length was about 16000 km while at 7:25:30 UT it was 18000 km; the apparent footpoint expansion velocity was about 5 km s^{-1}. The expansion was almost twice as big at Hα −0.8 Å.

Bunch *C* is the longest of all; it consists of at least two individual arches (Figs. 1, 2). The cloud velocity maps do not show the entire arch; in particular, the negative velocities region near the west footpoint is missing. Furthermore, they only show a very small portion of the second arch. The full system of motions is visible in the Doppler velocity maps (Fig. 4b), which show the classical type of motion and a smaller velocity gradient at the east footpoint than at the west, a remark that we made already for bunch *D*. The mass motions in the two arches of the bunch are different, thus the velocity gradient perpendicular to the axis is strong and results in extended zero velocity contours, almost parallel to the arch axis. There are no significant structural or velocity changes during the 13.5 min of our observations.

Bunch *B* initially consists of two arches (Figs. 1, 2). Again the cloud velocity maps do not show the entire arch, with the west footpoint missing in Fig. 4a. We note that the east footpoint of the arch is located next to a dark structure with strong negative velocities (Fig. 2), while the west footpoint is cospatial with the west footpoint of bunch *A*. The south arch of the bunch gradually fades and the north arch dominates (Fig 1a, 1f). Thirteen and a half minutes after the map of Fig. 3a (at 7:30:26, Fig. 5a) the cloud map shows negative velocities at the west footpoint. The positive velocity region of the bunch is somewhat shorter, the negative velocity region at both feet is enlarged and the negative velocities are larger. These changes are similar to those observed by Georgakilas et al. (1990, their bunch *I*).

An interesting case of arch filament formation was observed in bunch *A*, which appeared during our observing period. At 7:17:41 UT (Fig. 1b) it shows as a dark feature, about 8000 km long, near the west footpoint (closer to the center of the disk); subsequently the dark feature expanded towards the apex and further towards the other footpoint. At the end of our observations (after about 12.5 minutes) its length increased to about 18000 km (Fig. 1f), but it appears that it is not fully developed yet. The average apparent velocity of expansion was about 13.5 km s^{-1}. At 7:30:26 UT the mass motions associated with the arch were ascending near its leading edge (Fig. 5), the cloud velocity reaching 24 km s^{-1} and Doppler velocity 4 km s^{-1}. However the material at the footpoint was descending, as in the case of well developed AFS.

No cloud maps of the feature could be obtained in the early phase of its evolution. At 7:17:41 UT (time of Fig. 1b) we could only compute a Doppler map (Fig. 6a) which, again, shows descending material near the footpoint and ascending near the leading edge, with a peak velocity of 6 km s^{-1}. The material motions in this feature are also shown on the Doppler maps at

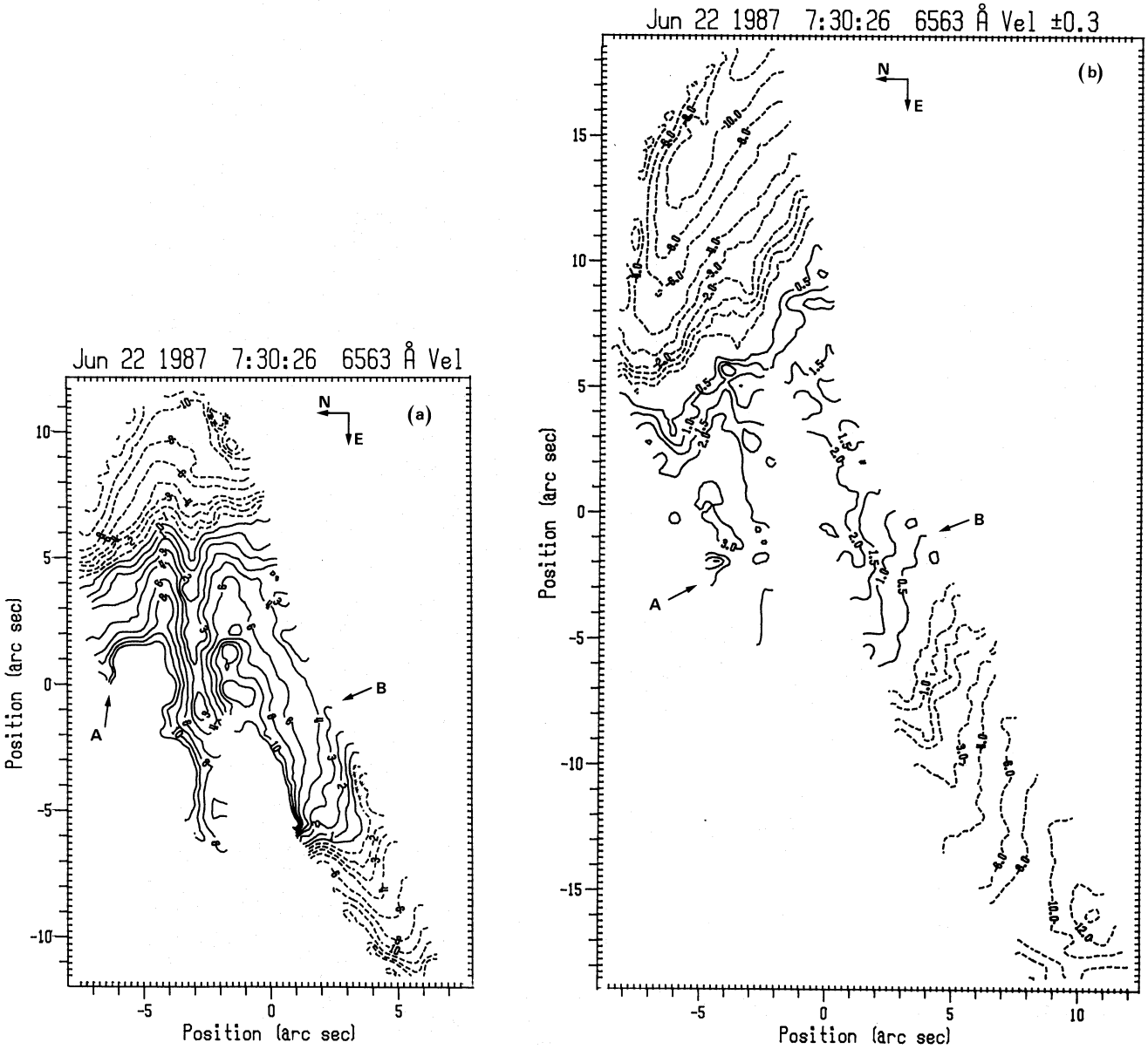

Fig. 5. Contour maps of cloud velocities (a) and Doppler velocities (b), at 7:30:26 UT

7:27:38 UT (Fig. 6b) and at 7:30:26 UT. Between the Doppler maps of 7:17:41 and 7:30:26 the zero velocity contour moved by about 4000 km, with an apparent speed of 5 km s^{-1}.

The presence of descending motions at the foot of the dark feature is in contradiction with its apparent expansion. One possible interpretation is that the expansion reflects changes in the physical conditions, rather than true material motion. On the other hand the shift of the zero velocity line and the decrease of the velocity between the two Doppler maps are signs of bulk motion, decelerating due to gravity. An alternative interpretation is that the material is ejected with a wide velocity range, so that the faster plasma is still rising while the slower plasma is falling due to the effects of gravity. It is interesting to note that the velocity structure of the developing AFS resembles that of flare associated ejection observed by Mein and Mein (1982) at the limb.

5. Reconstruction of the velocity vector

Using the method described by Georgakilas et al. (1990), we reconstructed the three-dimensional shape of the loop and the components of the velocity vector, assuming a plane, symmetric loop and a symmetric velocity field with respect to the apex. We applied this method to bunches *B* and *C* in 6 frames, covering a period of about 13.5 minutes and to bunch *D* in 4 frames, covering a period of 6.5 minutes (Table 1). The central axis of each bunch was estimated from maps computed by integrating the intensity over the Hα profile from Hα −0.8 Å to Hα +0.8 Å. In Table 2 we give the computed inclination angle β of the loop plane with respect to the vertical (positive values to the South), the height of the apex above the footpoints (measured on the plane of the AFS) with an accuracy of about 50% and the length of each bunch.

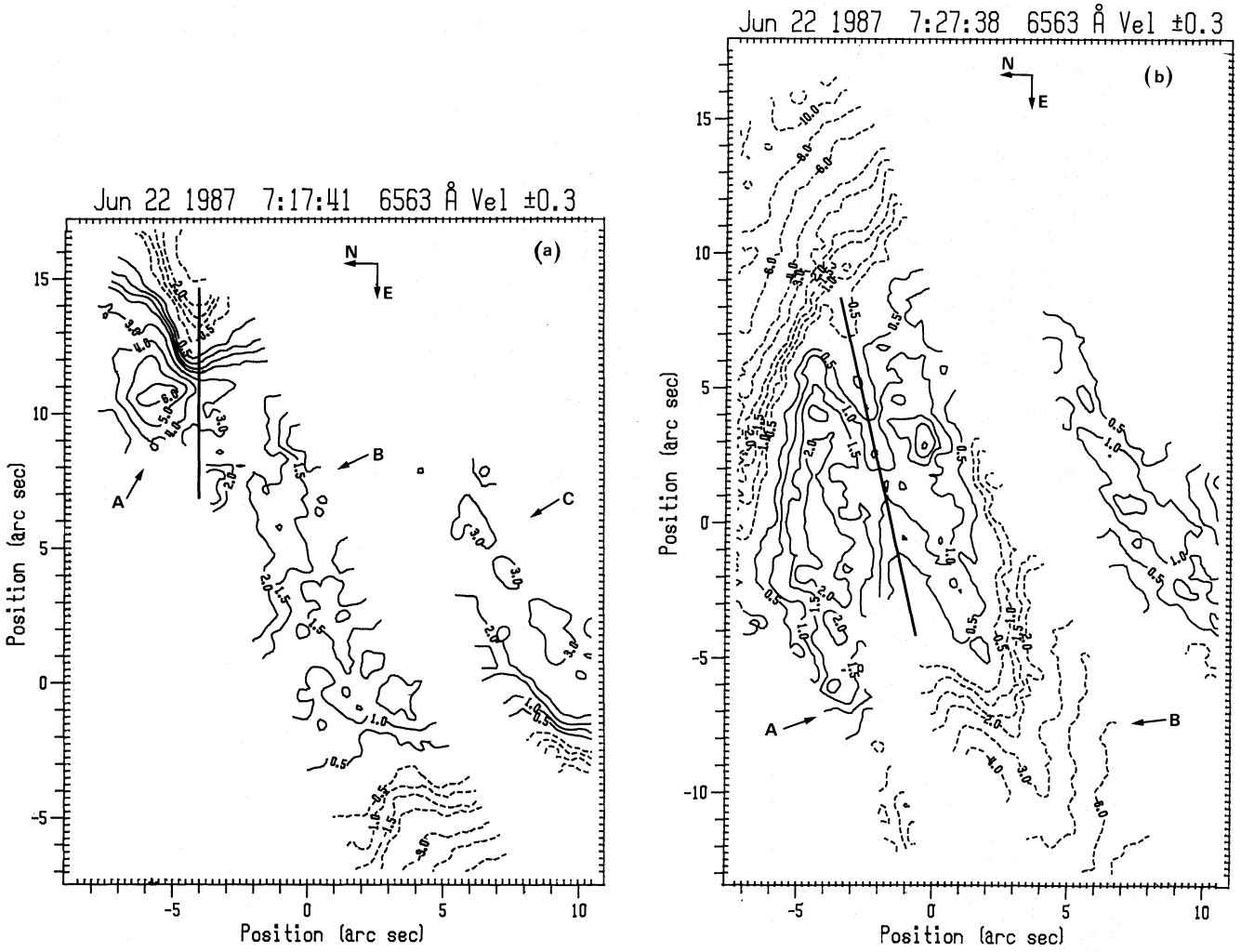

Fig. 6. Contour maps of Doppler velocities at 7:17:41 UT (a) and at 7:27:38 UT (b). The solid line separates bunch A from bunch B

Table 2. Inclination angle, height and length of AFS

Bunch	*B*	*C*	*D*
Inclination angle (°)	-30 ± 15	-40 ± 10	50 ± 10
Height (km)	2000	5500	4500
Length (km)	22000	31000	22000-27000

Bunches *B* and *C* did not show appreciable changes of their geometry during the 13.5 min that they were in the field of view. On the contrary bunch *D* showed an increase of his length (cf. section 4); our computations did not reveal any changes in the height of the bunch, which might be due to the limited accuracy. We note the relatively large inclination angles and also that this particular bunch is inclined in the opposite direction with respect to the others. This apparently reflects the inclination of the magnetic flux tubes, in the dipole-like magnetic field of the active region.

The components of the velocity vector for the three bunches are given in figure 7; they are averages of 6 frames for *B* and *C*, and 4 frames for *D*. Since in most cases the cloud maps did not show the entire arches we used the Doppler measurements at ± 0.3 Å for these computations. The horizontal component of the velocity is zero near the apex and its absolute value increases towards the footpoints, indicating transverse flow from the apex towards the footpoints. The perpendicular component on the plane of the loop has a maximum at the apex and strong negative values near the footpoints. Near the apex of arch *C* the velocity is about 5 km s^{-1} and about -22 km s^{-1} near the footpoints. For arch *B* the corresponding values are 2 km s^{-1} and -12 km s^{-1}, while for *D* they are almost 0 km s^{-1} and about -10 km s^{-1} respectively.

It is interesting to compare the above results with those computed with the cloud model. Such a comparison was possible for bunch *B* at 7:30:26 UT, for which the cloud model gave the velocity field along almost the entire arch. The results are given in figure 8. The Doppler shift method underestimates the horizontal component of the velocity by a factor of about two and the perpendicular component on the plane of the loop by more than a factor of five, near the footpoints (cf. section 4).

Within the error limit of the computation, the horizontal component of the velocity of bunches *B* and *C* showed no significant changes during the 13.5 minutes of our observations. The

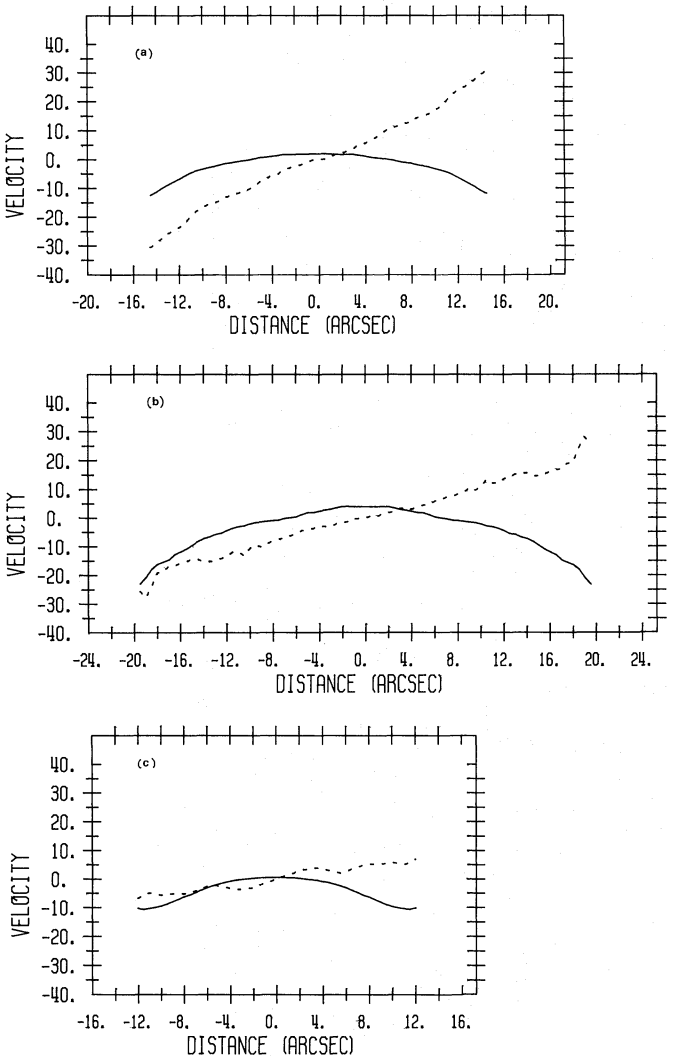

Fig. 7. Results of the computation of the velocity components from Doppler velocity measurements, assuming a symmetric loop and a symmetric velocity field. (a): bunch *B* (averaged over six frames, cf. Table 1); (b): bunch *C* (averaged over six frames); (c): bunch *D* (averaged over four frames). The solid line represents the perpendicular component on the loop plane and the dashed line the horizontal component. The velocity is in km s^{-1}

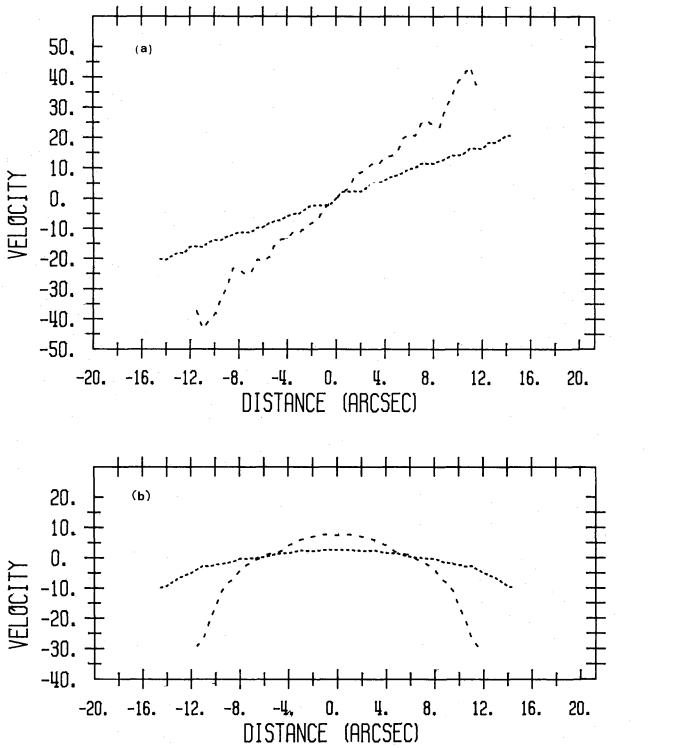

Fig. 8. Comparison of the velocity components along bunch *B* at 7:30:26 UT, computed from cloud velocities (dashed line) and Doppler velocities (dotted line); (a) shows the horizontal component and (b) the perpendicular component on the plane of the loop

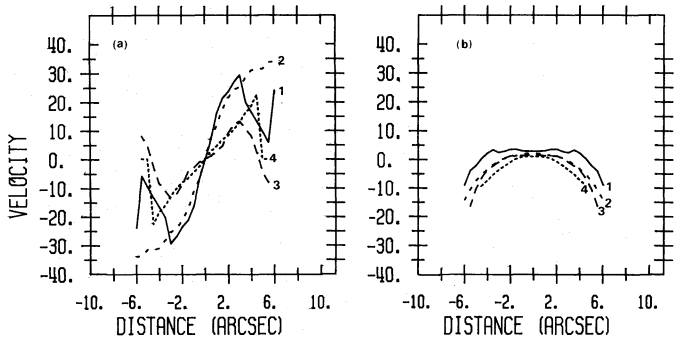

Fig. 9. Results of computation of the velocity components along bunch *D* (using cloud velocities) at 7:18:56 (1), 7:20:18 (2), 7:22:00 (3) and 7:25:30 (4); (a) is the horizontal and (b) the perpendicular component on the plane of the loop. We note that the arch expanded during our observations from about 22000 km to about 27000 km

same is true for the perpendicular component of the velocity. On the contrary, there were systematic changes in the velocity components of bunch *D*. For a better determination of the velocity components we used cloud velocities in a limited region near the apex (Fig. 9). The horizontal velocity decreased with time, while the perpendicular velocity decreased near the apex and increased to more negative values near the footpoints. Note the abrupt change in the horizontal velocity between the curves marked 1 and 2 and those marked 3 and 4 in Fig. 9a. Assuming that AFS represent rising flux tubes, the decrease of the velocity near the apex indicates a deceleration in the rise of the magnetic flux tube; this does not explain the increase of the downflow velocity near the footpoints, which is larger than the decrease near the apex. One possible interpretation is in terms of an upward stretch of the flux tube, so that the flow direction is closer to the vertical at the footpoints; this will also lead to a reduction of the horizontal velocity, in agreement with the observations.

6. Summary and conclusions

The Multichannel Double Pass Spectrograph (MSDP) provides sufficient spectral information in Hα, that can be used efficiently for studies of chromospheric structures with Beckers' cloud model. We have used the MSDP observations to compute physical parameters in arch filaments, with emphasis in the velocity field and its temporal evolution in conjunction with their morphology. Cloud maps show only the central parts of the arch filaments, which apparently satisfy the "high cloud" condition; Doppler maps show the entire arches but they provide no indication of their lateral boundaries. Both types of maps provide

useful information on the structure of the line of sight velocity; however, Doppler shift computations give lower velocity values.

Three of the four AFS bunches that we studied were fairly stable during our 15 min observing period and showed the well known velocity structure, with material rising near their apex and descending near their footpoints. The motion in the individual arches which compose the bunches show variations which can be strong and may result in extended zero velocity contours (e.g. bunch *C*). This in the case of limited resolution and small field of view may lead to wrong conclusions about the structure of the velocity field.

In agreement with Georgakilas et al. (1990) we found that, along the AFS axis, the velocity gradient is smaller near the limbward footpoint; we interpret this as the effect of horizontal flow from the apex to the footpoints. This was verified by reconstruction of the velocity vector, under the assumption of symmetry around the apex. From the Doppler maps we deduced horizontal velocities of up to 30 km s^{-1} near the footpoints, ascending motions not exceeding 5 km s^{-1} near the apex and descending motions up to 20 km s^{-1} at the footpoints. The corresponding cloud velocities were about 40 km s^{-1}, 10 km s^{-1} and 30 km s^{-1} respectively. These values are consistent with those derived by Georgakilas et al. (1990), on the basis of observations at Hα $\pm$.5 Å.

The reconstruction of the three-dimensional shape of the AFS showed that they were low structures, inclined some tens of degrees from the vertical, with the apex less than 5500 km above the footpoints (measured on the plane of the loop). We could not identify any height changes, probably due to the limited accuracy of the reconstruction; considering the value of the rising velocity and the inclination of the plane of the AFS, the change in the projected position should be less than 1000 km.

The large scale velocity structure did not change much during our observations, except for a small decrease of the positive velocity region around the apex and an increase of the negative velocity region at both feet (more prominent in bunch B). The reconstruction of the three dimensional shape and the components of the velocity in two AFS bunches (*B* and *C*) showed neither identifiable changes of their geometry nor systematic changes of the velocity vector along their axis. Bunch *D* showed an increase of its length, a decrease of its horizontal velocity, a decrease of the perpendicular velocity near the apex and a much greater increase to large negative values near the footpoints. This probably indicates a vertical stretching of the structure.

The fourth AFS bunch formed during our observations. It appeared as a darkening near one footpoint, subsequently it expanded towards the apex and further towards the other footpoint with an average velocity of about 13.5 km s^{-1}. The material motions of the arch (descending near the visible footpoint and ascending near the leading edge) were in contradiction with the picture of an expanding structure. Two interpretations are offered: either the apparent expansion reflects a change in physical conditions rather than true material motion, or the expanding plasma does not all start with the same speed, so that some material falls while the rest keeps rising. Whether it was material motion or not, this type of AFS formation departs from the idea that new arches are formed at low heights and become visible as the older ones expand and disappear (Frazier, 1972). The subject certainly deserves further investigation, with more observational data.

Acknowledgements. The authors are indebted to J. M. Malherbe, B. Schmieder, C. Coutard, R., Hellier for MSDP observations and C. Brechet for data processing. Travel funds for this work were provided in part through the bilateral scientific exchange program between France and Greece. The film was digitized with the fast microdensitometer MAMA of INSU (CNRS).

References

Alissandrakis C. E., Tsiropoula G., Mein P., 1990, A&A, 230, 200
Beckers J. M., 1964, Ph. D. Thesis, Utrecht
Bray R. J., 1973, Solar Phys., 29, 317
Bray R. J., 1974, Solar Phys., 38, 377
Bray R. J., Loughhead R. E., 1983, Solar Phys., 85, 131
Bruzek A., 1967, Solar Phys., 2, 451
Bruzek A., 1969, Solar Phys., 8, 29
Chou D.-Y., Wang H., 1987, Solar Phys., 110, 81
Chou D.-Y., Zirin H., 1988, ApJ, 333, 420
Frazier E. N., 1972, Solar Phys., 26, 130.
Gebbie K. B., Steinitz R., 1974, ApJ, 188, 399
Georgakilas A. A., Alissandrakis C. E., Zachariadis Th. G., 1990 Solar Phys., 129, 277
Grossmann-Doerth U., Von Uexkull M., 1971, Solar Phys., 20, 31
Grossmann-Doerth U., Von Uexkull M., 1973, Solar Phys., 28, 319
Grossmann-Doerth U., Von Uexkull M., 1977, Solar Phys., 55, 321
Mein P., 1977, Solar Phys., 54, 55
Mein P., 1991, A&A, 248, 669
Mein P., Mein N., 1982, Solar Phys., 80, 161
Roberts P. H., 1970, Ph. D. Thesis, Calif. Inst. Of Technology.
Steinitz R., Gebbie K. B., Bar V., 1977 ApJ, 213, 269
Zirin H., 1972, Solar Phys., 22, 34
Zwaan C., 1985, Solar Phys., 100, 397.

This article was processed by the author using Springer-Verlag LaTeX A&A style file 1990.